ACS APPLIED MATERIALS & INTERFACES

Research Article

www.acsami.org

Understanding Phase-Change Behaviors of Carbon-Doped $Ge_2Sb_2Te_5$ for Phase-Change Memory Application

Xilin Zhou,[†,‡,∥] Mengjiao Xia,[†,∥] Feng Rao,*[,†] Liangcai Wu,*[,†] Xianbin Li,*[,§] Zhitang Song,[†] Songlin Feng,[†] and Hongbo Sun[§]

[†]State Key Laboratory of Functional Materials for Informatics, Shanghai Institute of Micro-system and Information Technology, Chinese Academy of Sciences, Shanghai 200050, China

[‡]University of Chinese Academy of Sciences, Beijing 10080, China

[§]State Key Laboratory on Integrated Optoelectronics, College of Electronic Science and Engineering, Jilin University, Changchun 130012, China

ABSTRACT: Phase-change materials are highly promising for next-generation nonvolatile data storage technology. The pronounced effects of C doping on structural and electrical phase-change behaviors of $Ge_2Sb_2Te_5$ material are investigated at the atomic level by combining experiments and ab initio molecular dynamics. C dopants are found to fundamentally affect the amorphous structure of $Ge_2Sb_2Te_5$ by altering the local environments of Ge−Te tetrahedral units with stable C−C chains. The incorporated C increases the amorphous stability due to the enhanced covalent nature of the material with larger tetrahedral Ge sites. The four-membered rings with alternating atoms are reduced greatly with carbon addition, leading to sluggish phase transition and confined crystal grains. The lower RESET power is presented in the PCM cells with carbon-doped material, benefiting from its high resistivity and low thermal conductivity.

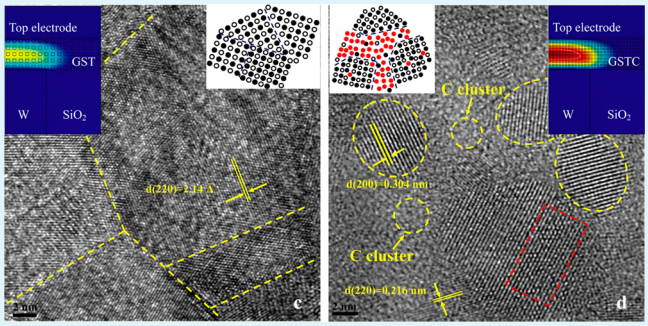

KEYWORDS: *phase-change material, $Ge_2Sb_2Te_5$, C doping, microstructure, molecular dynamic simulations, finite-element modeling*

INTRODUCTION

Phase-change technology is based on the rapid and reversible phase switching of chalcogenide alloys between high-resistive amorphous and low-resistive crystalline states. Phase-change optical storage has been highly commercialized for rewritable optical disks such as DVDs, and phase-change memory (PCM) is regarded as one of the leading contenders for the next-generation nonvolatile semiconductor memory due to its fast programming capability, high scalability, and low power requirement.[1] In the PCM cells, crystallization of the material arises when the amorphous region is heated above its crystallization temperature T_c by electrical pulses of low magnitude and long period (SET operation), while amorphization (i.e., RESET operation) is achieved by melting and quenching the active region with electrical pulses of higher magnitude and shorter duration.

$Ge_2Sb_2Te_5$ (GST) is a representative recording chalcogenide material in PCM cells that enables fast and stable phase transitions with high resistance resolution. In spite of the advantages over other material families, various researches have been devoted to tailoring the material properties of GST to improve the overall device performance. Among them, modified GST materials by doping Si,[2,3] N,[3−5] O,[6] and Ag[7] elements have usually been proposed to address the technical issues such as reducing the RESET current and suppressing the thermal inference in scaled device arrays. Recently, the reversible electrical switching of carbon-doped GST (GSTC) material has been reported,[8] in which the GSTC material with 18 at. % C content (GSTC18%) is emphasized due to the trade-off between the switching speed and thermal stability of PCM cells. The 10-year data retention temperature of GSTC18% is estimated to be 112 °C, which is drastically larger than that of GST (~89 °C). The carbon-doped phase-change material is also proposed as a good candidate material for the conformal deposition process, which is a key enablement to scale the confined device structure in high-density storage cells,[8,9] since C dopant can be incorporated from precursors and coreactants during deposition.[10] Because it is necessary to uniformly fill phase-change material in a confined cell with a high aspect ratio contact hole beyond 20 nm node using the film deposition process that offers good conformality, such as atomic-layer-deposition or metallorganic chemical vapor deposition.

It has been found that moderate C dopant in phase-change material is favored to increase the thermal stability, reduce the RESET current, and improve the device reliability.[9] Carbon

Received: June 4, 2014
Accepted: August 4, 2014
Published: August 4, 2014

dopant is also reported to significantly affect the atomic and electric structure of amorphous GST by using ab initio molecular dynamic (MD) simulations,[11,12] and the retarded crystallization process of the amorphous GSTC material is reported due to the decreased ABAB-type squared rings (with A as Ge or Sb and B as Te).[11] Even though, the mechanism of carbon action during the phase transition of the material is not very clear. It is essential to further provide detailed evidence about the role of carbon element in the atomic structure with reduced ABAB rings experimentally and theoretically. In this work, the intrinsic link between the improved phase-change properties and the bonding nature after C doping is elucidated by combining thin film analysis, device switching performance, finite-element modeling, and theoretical simulations. It is observed experimentally that the segregated amorphous carbon clusters during crystallization cause suppressed crystal grains and reduced thermal conductivity with embedded phase morphology. The incorporated C atoms contribute to the retarded phase transition process and enhanced thermal stability of the material by disordering the Ge−Te tetrahedral units, which is supported by the ab initio calculations. A slower switching speed with carbon addition is also confirmed by the practical device characterizations.

EXPERIMENTAL DETAILS

GST and GSTC films of 200 nm thickness are deposited on SiO_2/Si(100) substrate at room temperature by radio frequency magnetron cosputtering from stoichiometric GST and elemental C targets. The deposition proceeds with Ar at a flow rate of 50 SCCM (SCCM denotes cubic centimeter per minute at standard temperature and pressure) with the background pressure of 1×10^{-5} Pa. The C concentration in the film is determined by energy dispersive spectroscopy. The crystallization behavior is in situ studied using X-ray diffraction (XRD) in a PANalytical X'Pert PRO X-ray diffractomiter with Cu Kα radiation source. The diffraction data is collected over 2θ range of 20°−68° with an angular resolution of 0.025° as the films are heated in vacuum from room temperature to 400 °C at a rate of 40 °C/min. Data for every programmed temperature is obtained by stabilizing the temperature for 5 min. The room temperature Raman scattering spectra is recorded in a back scattering configuration. The 785 nm Ar ion laser is used as an excitation source. The incident laser power density is adjusted to low levels (~0.2 mW μm^{-2}) in order to avoid undesired structural deformation induced by absorption of high light intensity of laser, and the spectral resolution is ~1.2 cm^{-1}. The microstructure analysis of the films is carried out using transmission electron microscopy (TEM) and high-resolution TEM (HRTEM). For bright field (BF) TEM images and selected area electron diffraction (SAED) patterns, the 40 nm thick film is directly deposited on the carbon-coated supporting grids. To explore the electrical behavior of GSTC in memory cells, the PCM cells are fabricated with the traditional T-shaped (mushroom-type) structure using 0.13 μm complementary metal-oxide semiconductor technology. The diameter of the bottom W heat electrode is ~260 nm, which is covered by the GSTC film with ~100 nm thickness. The TiN (20 nm) and Al (300 nm) films are deposited as top electrodes. The PCM cells are patterned using etching process. The electrical characteristics of the PCM cells are evaluated by an arbitrary waveform generator (Tektronix AWG5002B) and a Keithley-2400 meter.

COMPUTATIONAL METHODS

The theoretical investigations in this work are performed employing the ab initio calculations based on the density functional theory. The Vienna Ab Initio Simulations Package is used for the first-principles MD calculations. The projector augmented wave pseudopotentials are used to describe electron−ion interactions. The generalized gradient approximation based on the Perdew−Burke−Ernzerhof (PBE) function is employed for the exchange-correlation energies between electrons. The energy cutoff for GSTC is chosen to be 520 eV, and 320 eV for GST. The k points of 2 × 2 × 2 is set for geometry optimization of models, while the Γ point is chosen for MD simulations, and a 3 fs time step is used.

To obtain amorphous properties of GSTC, melt-quench MD simulations are carried on 64 atoms supercells. The composition of GSTC is 14 C, 10 Ge, 10 Sb, and 25 Te atoms and 5 vacancies. The GST model for comparison contains 13 Ge, 13 Sb, 6 vacancies, and 32 Te atoms. These models are first melted at high-temperature 3000 K for 9 ps to make sure that they have lost the starting crystal character and then melted at 1200 K for 18 ps. Finally, the models are cooled to 300 K for 18 ps to reach amorphous state.

RESULTS AND DISCUSSION

Parts a and b of Figure 1 show the in situ measured XRD results of GST and GSTC18% film, respectively, with emphasis on the diffracted peaks in the 2θ range between 24° and 40°. Both of the films are amorphous as-deposited. In Figure 1a, the GST film crystallizes at around 160 °C, and the (200) peak of face centered cubic (FCC) phase appears with lattice parameter a of ~6.05 Å. For the GSTC film in Figure 1b, the crystallization begins at around 180 °C, with the lattice parameter a of FCC phase of ~6.20 Å. At higher temperature,

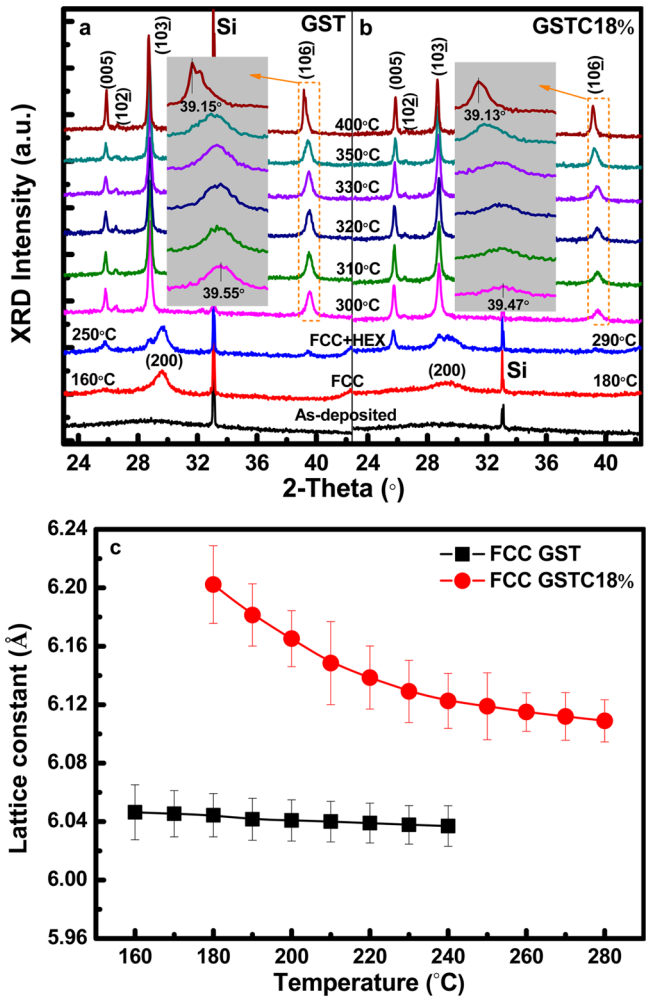

Figure 1. XRD peak intensity as a function of temperature at 40 °C/min for (a) GST and (b) GSTC18% films. The magnified hexagonal (106) peak is shown in the inset of the corresponding figures. (c) The lattice constant of FCC phase of the films as a function of temperature.

around 250 °C for GST film, and 290 °C for GSTC18% film, the diffracted peaks indexed to hexagonal (HEX) phase can be observed, revealing a FCC-HEX phase transition upon heating. It is obvious that the phase stability has been improved significantly for both the amorphous and FCC state of GSTC films. As the temperature increases up to 400 °C, the films retain the HEX structure with the (106) peak shifts toward the lower angle side gradually, which is due to the thermal expansion of the lattice. The quantitative variation of HEX lattice, *d*-spacing of (106) planes, of GSTC18% film (~0.83%) is smaller than that of GST material (~0.97%) as calculated from the corresponding peaks, which have been illustrated in the magnifying figures. This may be caused by one enhanced stressed rigid against thermal budgets for C doped material.[9] On the other hand, the evolution of lattice parameter of FCC phase with temperature is shown in Figure 1c, which indicates the behavior of C atoms during the crystallization process of the amorphous films. The lattice parameter of FCC GSTC18% film is considerably larger than that of FCC GST film, and the lattice parameter of the C-doped material decreases drastically as the temperature increases, in contrast to the relatively stable lattice parameter (around 6.04 Å) of GST material, as shown in the figure. This suggests that the incorporated C atoms are partially driven to grain boundaries upon crystallization, which may contribute to suppress the grains growth, while part of the C dopants are trapped in the crystal grains as interstitial or substitutional atoms, which leads to the increased lattice parameter.

The Raman spectra of the as-deposited, 250 °C-annealed, and 400 °C-annealed GST and GSTC films are given in the different panels of Figure 2, respectively. GSTC9% represents

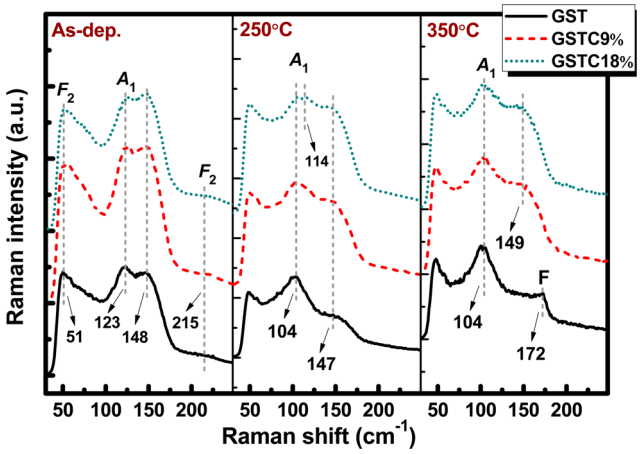

Figure 2. Raman scattering spectra of the GST, GSTC9%, and GSTC18% films. The spectra for the as-deposited (left panel), 250 °C-annealed (middle), and 350 °C-annealed (right panel) films are presented in the figure.

the GSTC material with C content of ~9 at. %. In the left panel of the figure, all the as-deposited films exhibit similar Raman spectra as a broad band covering 100–180 cm^{-1} frequency region with two overlapping bands peaking at ~123 cm^{-1} and ~148 cm^{-1}. The origin of the dominant Raman band at ~123 cm^{-1} is attributed to the symmetric stretching mode (A_1) of $GeTe_{4-n}Ge_n$ (n = 1, 2) corner-sharing tetrahedra,[13] while the latter Raman band at ~148 cm^{-1} is associated with Sb–Te bonds' vibrations in the $Sb–Te_3$ units.[14] The other Raman peaks at about 51 and 215 cm^{-1} can be more probably connected with the bending and antisymmetric stretching vibrational modes (F_2) of $GeTe_4$ tetrahedral, respectively.[13] It is noted that the intensity of Raman bands at 123 cm^{-1} decreases with richer C content as shown in the left panel, suggesting that the addition of carbon leads to a higher degree of disorder in the amorphous material by altering the local order around Ge–Te tetrahedral atoms. For the 250 °C-annealed films shown in the middle, a new Raman band peak can be observed at ~104 cm^{-1} instead of the peak at 123 cm^{-1} upon crystallization, which is related to A_1 mode of $GeTe_4$ corner-sharing tetrahedral,[13] and the broad peaks at ~147 cm^{-1} are preserved in the films. In GSTC18% film, however, a weak peak at ~114 cm^{-1} can be confirmed as marked in the figure, reminiscent of amorphous GSTC, revealing an enhanced thermal stability of its amorphous phase against microstructure ordering. The Raman band of Sb–Te vibrations in $SbTe_3$ units at ~148 cm^{-1} responds slightly to the crystallization from amorphous to FCC of the film since the local arrangement of atoms around Sb keeps unchanged on crystallization.[15] In other words, the rearrangement of Ge–Te network configuration is mainly responsible for the rapid phase-change of the amorphous phase,[16] since $GeTe_4$ tetrahedral is a crucial structural unit to be transformed to the distorted $GeTe_6$ octahedral in crystalline GST material.[13] Hence, the carbon atoms play a critical role in the GSTC alloy by disordering the Ge–Te network to postpone the crystallization procedure, which will be further discussed later. As the films are heated at 400 °C, as shown in the right panel, a new peak at ~172 cm^{-1} appears in the GST film accompanied by the disappearance of the peak at 148 cm^{-1}, which suggests the phase transformation from FCC to HEX. This indicates a significant variation in the local bonding distribution around Sb atoms in the GST film, which cannot be observed in the GSTC films due to the suppression of HEX phase by carbon atoms. A largely improved thermal stability of the FCC phase is therefore promised by carbon adding as reported before.[10] In addition, the Raman band profiles of the amorphous and FCC phase exhibit pronounced similarities whatever the carbon doping, revealing the existence of similar microstructural units.

The crystalline microstructures of the GST and GSTC18% films are analyzed in Figure 3 through TEM and HRTEM. The films are annealed at 250 and 400 °C, respectively, for 5 min. Figure 3a and b show the TEM BF images along with the associate selected area electron diffraction (SAED) patterns of the GST and GSTC18% films, respectively. The corresponding HRTEM images are presented in Figure 3c and d, respectively. It can be found from the images in Figure 3a and b that the grain size has been diminished considerably by carbon atoms. The SAED patterns in the insets are both assigned to FCC GST phase. The weaker diffraction contrast and less diffraction rings are confirmed in the carbon-doped film, indicating the restrained crystallization process thus better thermal stability of GSTC film which is consistent with the results discussed in Figures 1 and 2. In Figure 3c, the HRTEM image of GST film presents a polycrystalline structure with grains in tens of nanometer of size meeting and obstructing each other, as marked with dash lines in the figure. While for GSTC18% film, the HRTEM micrograph shown in Figure 3d clearly displays the smaller crystal grains (<10 nm) and the surrounding amorphous carbon cluster regions, as demonstrated with the dash rings. Smaller grain size of FCC phase is desired to improve the power, speed, and resistance drift performance of the highly scaled PCM devices.[17] The increased *d*-spacing (d_{220}

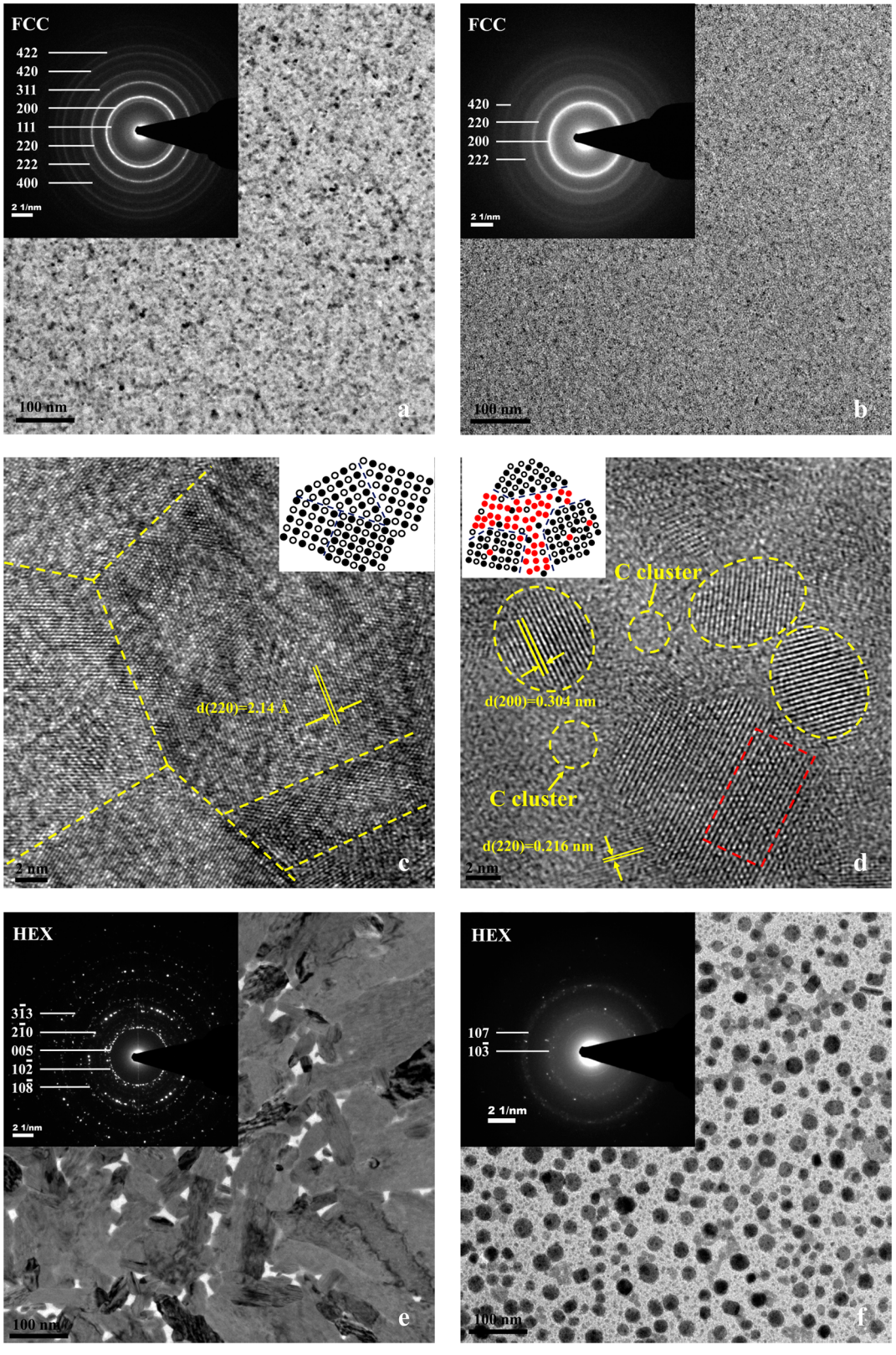

Figure 3. TEM BF images and the corresponding SAED patterns of the films: (a) FCC GST film; (b) FCC GSTC18% film; HRTEM images of (c) FCC GST and (d) FCC GSTC18% film, and schematic illustrations of corresponding crystalline phases in the insets; (e) HEX GST film; (f) HEX GSTC18% film.

= 2.16 Å) is obtained in FCC GSTC crystals with the larger lattice parameter of ~0.610 nm, which is good agreement with the XRD analysis. The lattice distortions over a few atomic distances can be identified in the dash rectangular area of Figure 3d, which is probably attributed to the incorporated carbon atoms trapped in the crystal grains as suggested in Figure 1. What's more, there is little evidence of crystallized carbon in Figure 3d, which reinforces the assumption that

dx.doi.org/10.1021/am503502q | ACS Appl. Mater. Interfaces 2014, 6, 14207−14214

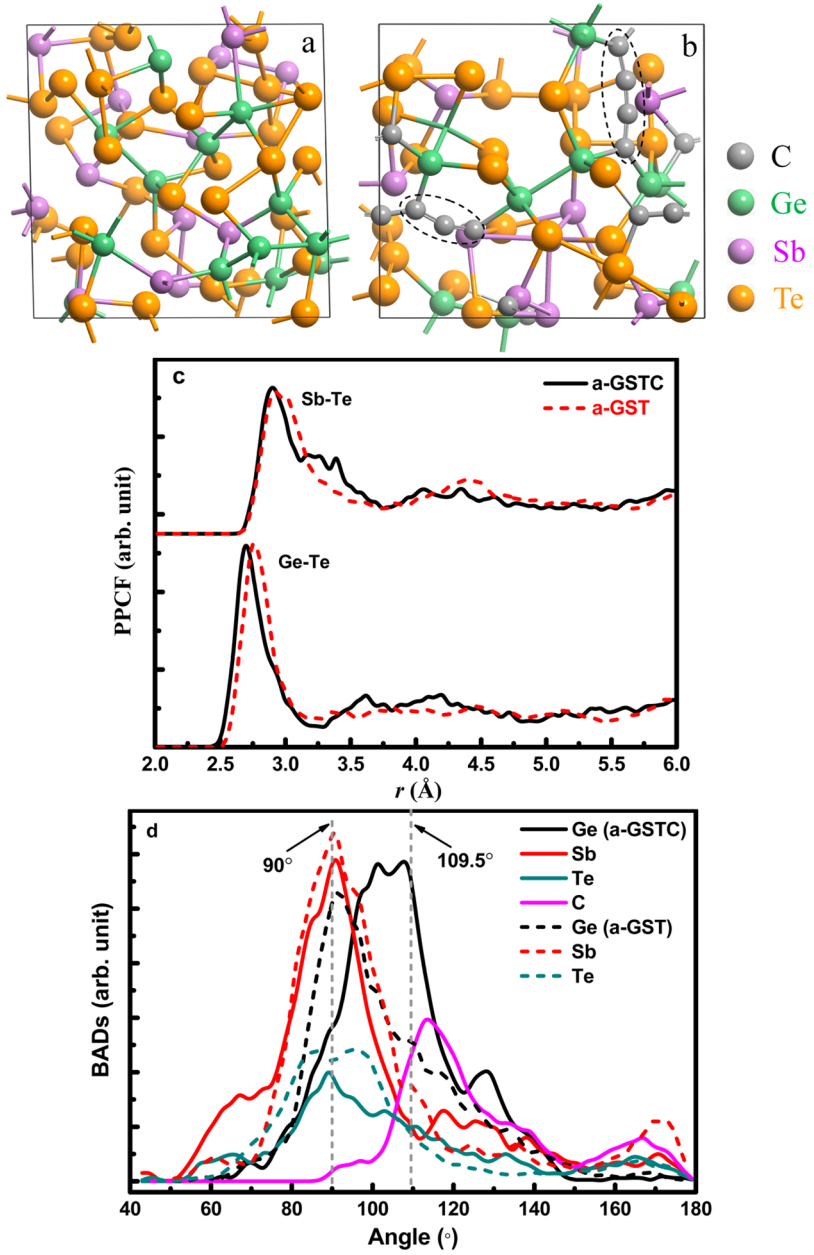

Figure 4. Amorphous structures of (a) GST and (b) GSTC at 300 K. (c) The PPCF of Sb−Te and Ge−Te. (d) The BAD around the atoms. The vertical dash lines indicate the octahedral (90°) and tetrahedral (109.5°) angles, respectively.

carbon atoms may partially accumulate in the amorphous matrix environing the reduced grain size. The contrast in microstructure morphology of the two materials is schematically illustrated in the insets in corresponding figures. For the films heated at 400 °C for 2 min, significant grain growth occurs as shown in Figure 3e and f for the GST and GSTC18% film, respectively, and the HEX crystal structure is identified from the SAED rings in the insets of the two figures. One of the most interesting features of the images in Figure 3e is the randomly distributed voids among the crystals as compared to the uniform phase morphology in Figure 3f with embedded bright and dark areas. The voids formation at high temperature is supposed to originate partly from the thermal induced transition to HEX structure and mainly from the evaporation of GST material.[18] The voids development cannot be observed in the GSTC18% film due to the enhanced thermal budget, which is beneficial for enhancing the cell reliability and enabling size scaling down architecture, since there are multichannel high-temperature (400 °C−410 °C) backend processes for PCM cell fabrication.

Theoretical simulations are performed to reveal the intrinsic origin of the local amorphous structures of the GST (a-GST) and GSTC (a-GSTC) materials. The computed melt-quenched amorphous structures of GST and GSTC are shown in Figure 4a and b, respectively. It is found that most carbon atoms exit in the form of C−Ge, C−Te, and C−C bonds with C−C chains as the most available structure, and the carbon atom in the sp^2-type triangular geometry is also identified with the presence of double bonds. It is noted that the C−C double bonds are observed in C−C chains as marked in the figure, which are formed during the melt-quench process, and keep very stable in the process of MD simulations in the liquid (1200 K). The presence of stable C−C chains with strong chemical bonds are supposed to be a factor that could account for larger network

dx.doi.org/10.1021/am503502q | ACS Appl. Mater. Interfaces 2014, 6, 14207−14214

Table 1. Structural Properties of Amorphous GST and GSTC[a]

	coordination numbers (avg. charge)				bond lengths (Å)		
	C	Ge	Sb	Te	Ge−Te	Sb−Te	4-fold rings
a-GST		4.26 (0.26)	3.57 (0.32)	2.87 (−0.23)	2.76	2.92	8 (5)
a-GSTC	2.60 (−0.40)	4.16 (0.47)	3.52 (0.49)	2.67 (−0.16)	2.68	2.91	5 (0)

[a]The numbers in parentheses in the last column indicate the population of ABAB rings.

rigidity thus higher thermal stability of the amorphous GSTC material,[19] which probably accumulate at the grains boundaries as cluster forms during the crystallization process, agreeing well with the in situ XRD analysis. The coordination numbers for Ge, Sb, Te, and C atoms that given in Table 1 are decreased in a-GSTC. This might be a consequence of considerable C−Ge and C−Te bonds, which would strengthen the covalent character of a-GSTC. The 4-fold ring structures of amorphous phases in Figure 4a and b are also considered in Table 1 with emphasis on ABAB rings that serve as nucleation site. The decrease of the 4-fold rings as well as the suppressed ABAB rings are confirmed in a-GSTC as reported before.[8] The reduced population of ABAB rings in a-GSTC is ascribed to the C−Ge(Te) bonds in the structure that connect to the C−C chains by interrupting the space continuity of ABAB rings, which should account for the sluggish nucleation and growth process of the material. On the other hand, the local structure of the amorphous models is investigated via partial pair correlation functions (PPCF) and bond angle distribution (BAD). The Ge/Sb−Te PPCF and BAD around the atoms is shown in Figure 4c and d, respectively. The Ge−Te bond length is found 0.08 Å shorter in a-GSTC, as summarized in Table 1. The peak position in the Ge-centered BAD significantly shifts to larger angle toward the tetrahedral angle (109.5°) in a-GSTC, indicating larger portion of tetrahedral Ge sites with C addition. The increased concentration of tetrahedral Ge leads to the reduction in the average Ge−Te bond length since the Ge−Te bond length in tetrahedral geometry is smaller than that in octahedral geometry. The increase in the concentration of tetrahedral Ge sites in a-GSTC causes the slower crystallization, since C might have restrained the transition of tetrahedral Ge sites into octahedral geometry. In Figure 4c and d, the effects of C incorporation in the Sb−Te PPCF and Sb-centered BAD are negligible, confirming that the configuration of octahedral geometry Sb atoms does not depend much on the C content, which is agreed with the results of the Raman spectra that C atoms mainly contribute to modify the local environment around Ge atoms. What's more, the average electronic charges on the atoms are estimated using Bader charge analysis as listed in Table 1,[20] in which both of the Te and C atomic charges are negative. It means that the C atoms are inclined to occupy the anion site (Te-site) rather than the cation site (Ge/Sb-site); that is, C dopants may partially substitute Te atoms in a-GSTC. Hence, the carbon dopants with C−C chains are found to significantly alter the amorphous structure by disordering the Ge−Te tetrahedral network, which will largely determine the electrical switching performances of the PCM cells.

The electrical program characteristics of PCM cells based on GST and GSTC films have been performed using pulsed measurements as plotted in Figure 5. The resistance−voltage curves of GST-, GSTC9%-, and GSTC18%-based PCM cells are shown in the different panels of Figure 5a with focus on the switching performance. The programming pulse width varies from 30 to 200 ns with the trailing edge of 10 ns. Note that the

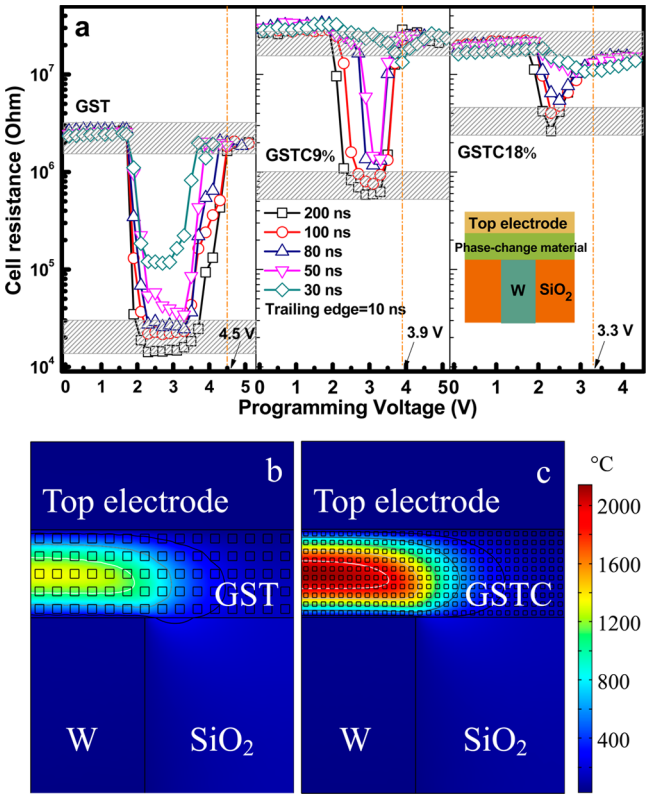

Figure 5. (a) Resistance−voltage characteristics of PCM cell using GST (left panel), GSTC9% (middle), and GSTC18% (right panel) materials at different voltage pulses. Simulated RESET temperature distributions in PCM cells with different grain sizes of (b) GST and (c) GSTC18% layers. Inset in part a is the schematics of the T-type cells. Each curve in part a is obtained from the statistical results of more than 10 PCM cells.

RESET state resistances of the PCM cells with GSTC are similar and increased by 1 order of magnitude compared to the undoped one, suggesting the larger localized states in amorphous GSTC materials, as revealed in the Raman spectra in Figure 2. For GST in the left panel of Figure 5a, a more conductive SET state is achieved with the resistance resolution of more than 2 orders of magnitude. In the case of GSTC9% in the middle of Figure 5a, a relatively slower crystallization switching is presented with resistance ratio of more than 1 order of magnitude for the pulse larger than 50 ns. It is obvious that a 30 ns pulse is sufficient to obtain such a resistance contrast for GST-based cells. While in the case of GSTC18% in the right panel, the resistance contrast decrease to several times for all pulse widths with the cell resistance of crystalline state being relatively high, and a pulse larger than 1000 ns is required to reach a SET state that is comparable to the one with 200 ns of the GSTC9%-based cell.[10] That is, for a given programming pulse width, the minimum achievable SET resistance tends to increase with carbon content, meaning that the crystallization

kinetics has been hampered increasingly by the growing carbon concentration. It is worth noting that the switching voltage is reduced widely with carbon doping in terms of RESET operation as marked in the figure. The RESET power diminution has been mainly ascribed to the improvement of thermal efficiency of the PCM cells, and the thermal conductivity and electrical resistivity are crucial factors to determine the thermal efficiency that governs power consumption of the PCM cells.[21] The thermal conductivity of crystalline GSTC18% film with smaller grains is determined to be around 0.2 W/mK by transient thermo-reflectance method, which is lower than that of FCC GST (0.6 W/mK).[21] The decreased thermal conductivity of the phase-change layer is correlated with the actual reduction of the active programmable volume caused by the accumulation of nanoclusters in the material,[21,22] as indicated by the TEM analysis and theoretical simulations. The calculated temperature contours of the GSTC- and GSTC18%-based PCM cells simulated for RESET are shown in Figure 5b and c, respectively, using a two-dimensional finite-element analysis, in which the grain size, thermal and electrical conductivity are smaller in GSTC layer than in GST layer. Constant pulse is applied to the axis-symmetric mushroom-type cells with tungsten plug. It is observed that the peak temperature in GSTC layer is much higher than that in GST layer, indicating that heat dissipation through the plug has been suppressed by the phase-change layer with high electrical resistivity and low thermal conductivity. Thus, lower RESET power is promised for the PCM cells with GSTC materials.

CONCLUSIONS

In summary, the influence of carbon addition in GST on phase stability and phase switching speed is investigated experimentally and theoretically. The experimental measurements present the enhanced structural stability of GSTC material both in amorphous and FCC phase by increasing the stressed rigid character of the material. During the crystallization process, the carbon dopants can be partially involved in the crystal units through disordering the Ge−Te network, and partially driven into the grain boundaries as cluster forms that suppress the grain size. The presence of carbon dopants with stable C−C chains is confirmed through ab initio calculations, which modifies the phase-change behavior of GSTC material greatly through breaking off the ABAB squared rings, resulting in retardant phase transition into crystalline state and confining the grain size. It is suggested that the substitutional carbon atoms are disposed to anionic configuration (Te atoms) in the amorphous network of GSTC. The electrical switching capability of the PCM cells is hindered by carbon adding in terms of switching speed and resistance contrast. The GSTC material with suppressed grains, high resistivity, and low thermal conductivity enables lower RESET power compared to GST, indicating a promising candidate material for low-power PCM application.

AUTHOR INFORMATION

Corresponding Authors

*Email: fengrao@mail.sim.ac.cn.
*Email: wuliangcai@mail.sim.ac.cn.
*Email: lixianbin@jlu.edu.cn.

Author Contributions

[‖]X.Z. and M.X. contributed equally to this work.

Notes

The authors declare no competing financial interest.

ACKNOWLEDGMENTS

This work is Supported by National Key Basic Research Program of China (2011CBA00607, 2013CBA01902, 2010CB934300), Strategic Priority Research Program of Chinese Academy of Sciences (XDA09020402), National Integrate Circuit Research Program of China (2009ZX02023-003), Science and Technology Council of Shanghai (11DZ2261000), National Natural Science Foundation of China (11104109, 11374119). The author X. Zhou is thankful for the financial support of the CAS Special Grant for Postgraduate Research, Innovation, and Practice. The supercomputer time was provided by HPCC at JLU.

REFERENCES

(1) Lankhorst, M. H. R. B.; Ketelaars, W.; Wolters, R. A. M. Low-cost and Nanoscale Nonvolatile Memory Concept for Future Silicon Chips. *Nat. Mater.* **2005**, *4*, 347−352.
(2) Kölpin, H.; Music, D.; Laptyeva, G.; Ghadimi, R.; Merget, F.; Richter, S.; Mykhaylonka, R.; Mayer, J.; Schneider, J. M. Influence of Si and N Additions on Structure and Phase Stability of $Ge_2Sb_2Te_5$ Thin Films. *J. Phys.: Condens. Matter* **2009**, *21*, 435501.
(3) Cho, E.; Han, S.; Kim, D.; Horii, H.; Nam, H. S. Ab Initio Study on Influence of Dopants on Crystalline and Amorphous $Ge_2Sb_2Te_5$. *J. Appl. Phys.* **2011**, *109*, 043705.
(4) Kim, Y.; Jang, M. H.; Jeong, K.; Cho, M.-H.; Do, K. H.; Ko, D.-H.; Sohn, H. C.; Kim, M. G. Investigation of Phase Transition of $Ge_2Sb_2Te_5$ and N-Incorporated $Ge_2Sb_2Te_5$ Films Using X-ray Absorption Spectroscopy. *Appl. Phys. Lett.* **2008**, *92*, 061910.
(5) Shelby, R. M.; Raoux, S. Crystallization Dynamics of Nitrogen-Doped $Ge_2Sb_2Te_5$. *J. Appl. Phys.* **2009**, *105*, 104902.
(6) Song, K. B.; Sohn, S. W.; Kim, J.; Kim, K. A.; Cho, K. Chalcogenide Thin-Film Transistors Using Oxygenated N-type and P-type Phase Change Materials. *Appl. Phys. Lett.* **2008**, *93*, 043514.
(7) Prasai, B.; Chen, G.; Drabold, D. A. Direct Ab Initio Molecular Dynamic Study of Ultrafast Phase Change in Ag-Alloyed $Ge_2Sb_2Te_5$. *Appl. Phys. Lett.* **2013**, *102*, 041907.
(8) Zhou, X.; Wu, L.; Song, Z.; Rao, F.; Zhu, M.; Peng, C.; Yao, D.; Song, S.; Liu, B.; Feng, S. Carbon-Doped $Ge_2Sb_2Te_5$ Phase Change Material: A Candidate for High Density Phase Change Memory Application. *Appl. Phys. Lett.* **2012**, *101*, 142104.
(9) Beneventi, G. B.; Perniola, L.; Sousa, V.; Gourvest, E.; Maitrejean, S.; Bastien, J. C.; Bastard, A.; Hyot, B.; Fargeix, A.; Jahan, C.; Nodin, J. F.; Persico, A. Carbon-doped GeTe: A Promising Material for Phase-Change Memories. *Solid-State Electron.* **2011**, *65−66*, 197−204.
(10) Zheng, J. F.; Reed, J.; Schell, C.; Czubatyj, W.; Sandoval, R.; Fournier, J.; Li, W.; Hunks, W.; Dennison, C.; Hudgens, S.; Lowrey, T. MOCVD $Ge_3Sb_2Te_5$ for PCM Applications. *IEEE Electron Device Lett.* **2010**, *31*, 999−1001.
(11) Cho, E.; Youn, Y.; Han, S. Enhanced Amorphous Stability of Carbon-Doped $Ge_2Sb_2Te_5$: Ab Initio Investigation. *Appl. Phys. Lett.* **2011**, *99*, 183501.
(12) Borisenko, K. B.; Chen, Y. X.; Cockayne, D. J. H.; Song, S. A.; Jeong, H. S. Understanding Atomic Structures of Amorphous C-doped $Ge_2Sb_2Te_5$ Phase-Change Memory Materials. *Acta Mater.* **2011**, *59*, 4335−4342.
(13) Andrikopoulos, K. S.; Yannopoulos, S. N.; Voyiatzis, G. A.; Kolobov, A. V.; Ribes, M.; Tominaga, J. Raman Scattering Study of The a-GeTe Structure and Possible Mechanism for the Amorphous to Crystal Transition. *J. Phys.: Condens. Matter* **2006**, *18*, 965−979.
(14) Watanabe, I.; Noguchi, S.; Shimizu, T. Study on Local Structure in Amorphous Sb−S Films by Raman Scattering. *J. Non-Cryst. Solids* **1983**, *58*, 35−40.

(15) Kolobov, A. V.; Fons, P.; Frenkel, A. I.; Ankudinov, A. L.; Tominaga, J.; Uruga, T. Understanding the Phase-Change Mechanism of Rewritable Optical Media. *Nat. Mater.* **2004**, *3*, 703−708.
(16) Kolobov, A. N.; Fons, P.; Tominaga, J. Phase-Change Optical Recording: Past, Present, Future. *Thin Solid Films* **2007**, *515*, 7534−7537.
(17) Wang, W.; Loke, D.; Law, L.; Shi, L.; Zhao, R.; Li, M.; Chen, L.; Yang, H.; Yeo, Y.; Adeyeye, A.; Chong, T.; Lacaita, A. Engineering Grains of $Ge_2Sb_2Te_5$ for Realizing Fast-Speed, Low-Power, and Low-Drift Phase-Change Memories with Further Multilevel Capabilities. *IEDM Technol. Dig.* **2012**, 31.3.1−31.3.4.
(18) Cheng, H. Y.; Hsu, T. H.; Raoux, S.; Wu, J. Y.; Du, P. Y.; Breitwisch, M.; Zhu, Y.; Lai, E. K.; Joseph, E.; Mittal, S.; Cheek, R.; Schrott, A.; Lai, S. C.; Lung, H. L.; Lam, C. A High Performance Phase Change Memory with Fast Switching Speed and High Temperature Retention by Engineering the $Ge_xSb_yTe_z$ Phase Change Material. *IEDM Technol. Dig.* **2011**, 3.4.1−3.4.4.
(19) Micoulaut, M.; Raty, J.-Y.; Otjacques, C.; Bichara, C. Understanding Amorphous Phase-Change Materials from the Viewpoint of Maxwell Rigidity. *Phys. Rev. B* **2010**, *81*, 174206.
(20) Skelton, J. M.; Lee, T. H.; Elliott, S. R. Structural, Dynamical, and Electronic Properties of Transition Metal-doped $Ge_2Sb_2Te_5$ Phase-change Materials Simulated by Ab Initio Molecular Dynamics. *Appl. Phys. Lett.* **2012**, *101*, 024106.
(21) Lee, T.-Y.; Kim, K. H. P.; Suh, D.-S.; Kim, C.; Kang, Y.-S.; Cahill, D. G.; Lee, D.; Lee, M.-H.; Kwon, M.-H.; Kim, K.-B.; Khang, Y. Low Thermal Conductivity in $Ge_2Sb_2Te_5$−SiO_x for Phase Change Memory Devices. *Appl. Phys. Lett.* **2009**, *94*, 243103.
(22) Morikawa, T.; Akita, K.; Ohyanagi, T.; Kitamura, M.; Kinoshita, M.; Tai, M.; Takaura, N. A Low Power Phase Change Memory Using Low Thermal Conductive Doped-$Ge_2Sb_2Te_5$ with Nano-Crystalline Structure. *IEDM Technol. Dig.* **2012**, 31.4.1−31.4.4.

NOTE ADDED AFTER ASAP PUBLICATION

This paper was published on the Web on August 14, 2014. The last co-author on the paper, S. B. Zhang, was removed from the paper, and the corrected version was reposted on August 18, 2014.